L. Xiang, M. Zhang, and A. Klein, “Robust Dynamic Trajectory Optimization for UAV-aided Localization of Ground Target”, in *IEEE Global Communications Conference (Globecom)*, Kuala Lumpur, Malaysia, Dec. 2023.

Robust Dynamic Trajectory Optimization for UAV-aided Localization of Ground Target

Lin Xiang, Mengshuai Zhang, and Anja Klein
Communications Engineering Lab, Technical University of Darmstadt, Darmstadt, Germany
Email: {l.xiang, a.klein}@nt.tu-darmstadt.de, mengshuai.zhang@stud.tu-darmstadt.de

***Abstract*—In this paper, we consider employing an unmanned aerial vehicle (UAV) equipped with an onboard radar transceiver to localize a ground target at an unknown position. Exploiting the UAV's mobility, we aim to gather line-of-sight (LoS) range measurements from favorable waypoints and improve the ensuing multi-lateration process while estimating the target's location. To this end, we introduce a novel localization error metric, characterized geometrically by the radius of a defined confidence region where the target resides at a predetermined confidence level. Additionally, we investigate robust dynamic optimization of the UAV's trajectory to minimize the defined localization error metric *online*, utilizing sequentially available but delayed range estimates. The formulated optimization problem belongs to a convex-nonconcave minimax problem, which is generally intractable. To solve this problem, we further propose two iterative online algorithms based on semidefinite programming (SDP) relaxation and alternating/sequential convex optimization techniques. Simulation results show that the proposed online schemes outperform several benchmarks, either in the final localization accuracy or in the rate of decreasing the localization error.**

I. Introduction

The utilization of unmanned aerial vehicles (UAVs) for localizing ground targets has recently attracted significant interest [1], especially in applications such as search-and-rescue operations in emergency scenarios [2]. Thereby, elevated UAVs can enable line-of-sight (LoS) propagation of sensing signals to ground targets, to effectively mitigate bias in range measurements [3]. Moreover, UAVs can be fast deployed and flexibly relocated to favorable positions during range measurement, which further reduces the region of localization uncertainty in the ensuing multi-lateration process [7]. However, how to plan the UAV's flight path/trajectory, namely the sequence of waypoints and velocities, to achieve high-precision high-accuracy localization remains a prominent research concern.

So far, the existing literature has explored both static [4], [6] and dynamic [8], [9] path planning schemes for UAV-aided localization. In static path planning, trajectories are usually predetermined based on heuristics, such as to explore the residing area of ground targets from diverse positions or angles [4]. At each predetermined waypoint, the UAVs collect key metrics like time-of-arrival (TOA), time-difference-of-arrival (TDOA), or received-signal-strength (RSS) [5]. These data points indicate the ranges of the ground targets, which are then combined for final position estimation [6]. While the static path planning is simple to implement, it may consume substantial amounts of time and energy in order to achieve a desired localization performance. Conversely, dynamic path planning, which determines the next waypoints of the UAVs in real-time based on range or position estimates available *online* [8], [9], potentially promises superior localization performance. However, due to inherent noise in range measurements and uncertainties around target positions, it is challenging to predict the localization performance at given waypoints, before flying to these waypoints and collecting new range estimates there. For example, the offline metrics such as the mean squared error (MSE) and Cramér-Rao lower bound (CRLB) [8] cannot be directly used for the online setting as they depend on the unknown target positions.

Therefore, several research questions need to be urgently addressed for dynamic path planning, including *(i) how to model the localization error as a cost function of UAV's next waypoint* that captures the impact of both measurement noise and the underlying geometry, e.g., the relative positions between UAVs and ground targets, during multi-lateration and *(ii) how to optimize the UAV's trajectory online*. In [9], the authors proposed to approximate the target position in CRLB by its real-time estimate and used the resulting approximate CRLB together with maximum likelihood position estimation [10] for dynamic path planning. However, the approach lacks guarantee on the performance achievable in practical settings, as it eventually minimizes a lower bound of localization error.

Unlike the existing literature [8], [9], this paper investigates dynamic path planning for UAV-aided localization by employing a robust optimization approach. We first propose a novel localization error metric, defined by the radius of an α-confidence region of localization, to capture a (probabilistic) upper bound on localization error. Then, we consider online optimization of UAV's next waypoints for minimization of the proposed error metric. We formulate an intractable convex-nonconcave minimax optimization problem, and further propose two online low-complexity iterative algorithms to solve it. Our robust optimization approach is inspired by the wireless sensor network aided localization approach considered in [11], but it has significantly extended the latter in order to enable trajectory optimization for UAV-aided localization under random range errors. Our contributions are:

- We propose a robust minimax approach, using a novel localization error metric defined based on the α-confidence region of localization, tailored for trajectory optimization in UAV-aided localization of ground target.
- We formulate a nonconvex minimax trajectory planning problem for minimization of the defined localization error metric. To solve the intractable problem, we fur-

This work has been funded by the LOEWE initiative (Hesse, Germany) within the emergenCITY center and has been supported by the BMBF project Open6GHub under grant 16KISKO14 and by DAAD with funds from the German Federal Ministry of Education and Research (BMBF).

ther propose two iterative online algorithms based on semidefinite programming (SDP) relaxation together with alternating convex optimization (ACO)/successive convex approximation (SCA).

- Simulation results show that the proposed online algorithm based on SDP and ACO outperforms in localization accuracy, while the other proposed algorithm exhibits accelerated rates in reducing the localization error.

Notation: Throughout this paper, $\mathbb{R}$, $\mathbb{R}^N$, and $\mathbb{R}^{N\times M}$ denote the set of real numbers, $N \times 1$ vectors, and $N \times M$ matrices, respectively. $\mathbf{I}_N$ is the $N \times N$ identity matrix. $(\cdot)^{\mathrm{T}}$ and $\mathrm{Tr}(\cdot)$ are the transpose and trace of matrices, respectively. $\Pr(\cdot)$ is the probability operator. $\mathcal{P}_{\mathcal{C}}(\cdot)$ denotes the projection operator onto set $\mathcal{C}$. $|\cdot|$ and $\|\cdot\|$ denote the absolute value of a scalar and ℓ_2-norm of a vector. Finally, $\nabla f(\cdot)$ (or $\nabla_{\mathbf{x}} f(\cdot)$) is the gradient of function $f(\cdot)$ (with respect to $\mathbf{x}$).

II. System Model

A. UAV-aided Localization of Ground Target

As shown in Fig. 1, we consider a rotary-wing UAV equipped with a full-duplex radar transceiver to localize a terrestrial target by patrolling over a rectangular area of dimension $L_{\mathrm{x}} \times L_{\mathrm{y}}$. We assume that the target remains static and its position $\mathbf{p}_{\mathrm{s}} = (x_{\mathrm{s}}, y_{\mathrm{s}})^{\mathrm{T}} \in \mathbb{R}^2$ is unknown to the UAV.

The UAV chooses N waypoints at a fixed altitude h for range measurement. The value of N is specified a priori according to e.g. the time and energy budgets of the mission and the UAV. Let $\mathbf{u}_n = (x_n, y_n)^{\mathrm{T}} \in [0, L_{\mathrm{x}}] \times [0, L_{\mathrm{y}}]$ be the ground position of the UAV's nth waypoint for $n \in \{1, 2, \ldots, N\}$, and $\mathbf{u}_0$ be the initial waypoint. We assume that the UAV flies in a straight line from $\mathbf{u}_{n-1}$ to $\mathbf{u}_n$ for a duration of Δ_{f}. Furthermore, at each waypoint, the UAV hovers for a duration Δ_{h} to collect range measurements. We define $\Delta = \Delta_{\mathrm{h}} + \Delta_{\mathrm{f}}$.

The UAV employs the two-way ToA method [12] for range measurement. Thereby, while hovering at waypoint $\mathbf{u}_n$, the UAV broadcasts radar sensing signals, detects and receives the echos of sensing signals reflected by the target, and estimate the two-way propagation delay of the received echoes using e.g. the maximum-likelihood estimation. As the UAV is elevated, we assume that the sensing signal propagates over LoS path to the target. Moreover, for convenience of presentation, we assume that self-interference in the radar transceiver is negligible. Let P be the transmit power of the UAV. The received signal-to-noise ratio (SNR) is given by

$$\mathrm{SNR}_n = \frac{\beta \cdot P}{\sigma^2 \cdot (d_n)^4}, \tag{1}$$

where σ^2 is the noise power at the receiver. β is a power-gain factor given by $\beta = G_{\mathrm{T}} \cdot G_{\mathrm{R}} \cdot \sigma_{\mathrm{rcs}} \cdot \lambda^2/(4\pi)^3$, where G_{T} and G_{R} are the transmit and receive antenna gain of the UAV, respectively, σ_{rcs} is the radar cross-section (RCS) of the target [13], and λ is the signal wavelength.

Let τ_n be the (two-way) runtime of the sensing signal. The range between the UAV and the target is given by

$$d_n = \sqrt{h^2 + ||\mathbf{u}_n - \mathbf{p}_{\mathrm{s}}||^2} = c \cdot \tau_n/2, \tag{2}$$

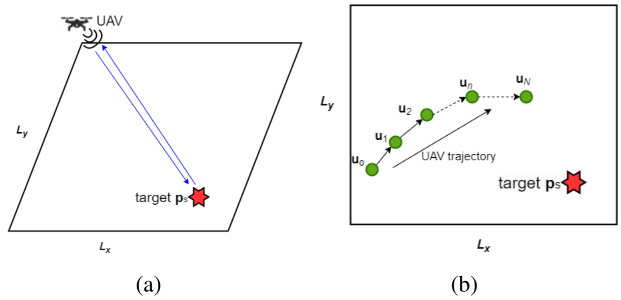

Fig. 1: Illustration of (a) UAV-aided localization at waypoint $\mathbf{u}_n$ and (b) UAV trajectory projected on the ground.

where c is the speed of light. Due to impairment of e.g. noise at the radar receiver, the runtime τ_n and range d_n is usually imperfectly estimated in practice [14].The range estimate, denoted by $\hat{d}_n$, is modeled as

$$\hat{d}_n = d_n + \epsilon_n, \tag{3}$$

where ϵ_n is the random measurement error. Based on the radar literature [13], ϵ_n follows a Gaussian distribution with zero mean and variance σ_n^2 that is inversely proportional to the SNR of received echo signal, i.e.,

$$\sigma_n^2 = \frac{a}{\mathrm{SNR}_n} = \frac{a \cdot \sigma^2}{\beta \cdot P} \cdot (d_n)^4. \tag{4}$$

Here, a is a constant whose value depends on the waveform of sensing signal and the runtime estimation algorithm.

B. α-Confidence Region of Localization

The range estimate $\hat{d}_n$ in (3) follows a Gaussian distribution with unbounded support and its mean and variance are both unknown. Hence, the conventional region of localization uncertainty, namely the set of all possible locations of the target inferred based on the available range measurements, is also unbounded, which cannot be directly used for robust optimization. To tackle this challenge, here we propose a novel localization error metric, referred to as the α-confidence region of localization. The metric characterizes a subset of the region of localization uncertainty in which the target lies with confidence level $\alpha \in (0, 1]$. In this paper, α is specified a priori, but can be fine-tuned to improve the localization performance.

Assume that the UAV obtains M range measurements $\hat{d}_{n,m}$, $m = 1, ..., M$, at waypoint n, whose sample mean $\overline{d}_n$ and sample variance $\hat{\sigma}_n^2$ are calculated as

$$\overline{d}_n = \frac{1}{M} \sum\nolimits_{m=1}^{M} \hat{d}_{nm}, \tag{5}$$

$$\hat{\sigma}_n^2 = \frac{1}{M-1} \sum\nolimits_{m=1}^{M} (\hat{d}_{nm} - \overline{d}_n)^2. \tag{6}$$

According to [14], the random variable defined by $(\overline{d}_n - d_n)/(\sqrt{\hat{\sigma}_n^2/M})$ follows the t-distribution with $(M-1)$ degrees of freedom. Thus, we have

$$\Pr\left\{\overline{I}_n \leq d_n \leq \overline{O}_n\right\} = \alpha. \tag{7}$$

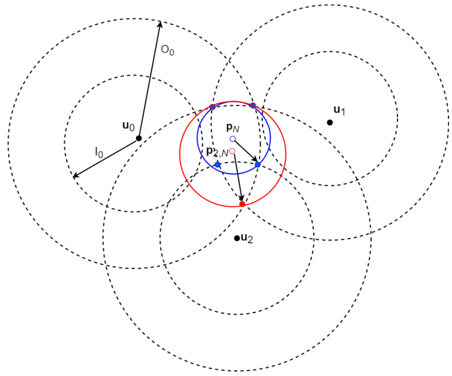

Fig. 2: Confidence region of localization (with blue vertices/extreme points) and its Chebyshev circle with/without inner range constraints (in blue/red solid line).

i.e., $[\overline{I}_n, \overline{O}_n]$ is an α-confidence interval for d_n, with

$$\overline{I}_n = \overline{d}_n - t_{1-\alpha}\hat{\sigma}_n/\sqrt{M}, \tag{8a}$$

$$\overline{O}_n = \overline{d}_n + t_{1-\alpha}\hat{\sigma}_n/\sqrt{M}. \tag{8b}$$

Here, $t_{1-\alpha}$ is the critical t-value for $1-\alpha$ and can be looked up in the t-table. Note that as $M \to \infty$, we have $\overline{d}_n \to d_n$, $\hat{\sigma}_n^2 \to \sigma_n^2$, and the distribution of random variable $(\overline{d}_n - d_n)/(\sqrt{\hat{\sigma}_n^2/M})$ approaches normal.

Let $I_n = \sqrt{\overline{I}_n^2 - h^2}$ and $O_n = \sqrt{\overline{O}_n^2 - h^2}$. Substituting (2) into (7), the α-confidence region of localization, the term being borrowed from the α-confidence interval for d_n, after having measured at N waypoints is defined as

$$\mathcal{S}_N \triangleq \left\{ \mathbf{s} \in \mathbb{R}^2 \,|\, I_n \leq \|\mathbf{u}_n - \mathbf{s}\| \leq O_n,\ n = 0, 1, \ldots, N \right\}. \tag{9}$$

As illustrated in Fig. 2, $\mathcal{S}_N$ is the intersection of disks centered at each waypoint $\mathbf{u}_n$, where the inner and outer radii of each disk are given by I_n and O_n, respectively. Assume that (7) holds for $N+1$ waypoints well dispersed in different directions from the target. We can estimate that $\Pr\{\mathbf{p}_\mathrm{s} \in \mathcal{S}_N\} = \Pr\{d_n \in [\overline{I}_n, \overline{O}_n], n = 0, 1, \ldots, N\} \approx 1-(1-\alpha)^{N+1}$; but the converse is not true. This further implies $\Pr\{\mathbf{p}_\mathrm{s} \in \mathcal{S}_N\} \to 1$ when N is large enough, provided $\alpha \in (0, 1]$.

Now, consider the minimum circle enclosing the confidence region $\mathcal{S}_N$, i.e., the Chebyshev circle of $\mathcal{S}_N$ [11], cf. Fig. 2. The center and radius of the Chebyshev circle of $\mathcal{S}_N$, denoted as $\mathbf{p}_N$ and R_N, can be obtained by

$$(\mathbf{p}_N, R_N) = \underset{(\mathbf{p}, R)}{\operatorname{argmin}} \left\{ R^2 \,|\, \|\mathbf{s} - \mathbf{p}\| \leq R, \forall \mathbf{s} \in \mathcal{S}_N \right\}. \tag{10}$$

Here, $\mathbf{p}_N$ provides a convenient estimate of the target location and R_N is the resulting minimum worst-case localization error with given probability. As $\mathcal{S}_N$ is a nonconvex set, the position estimate may lie out of $\mathcal{S}_N$. However, for UAV-aided localization, the likelihood can be reduced by optimizing the waypoints.

III. Robust Offline Trajectory Optimization

Sec. II reveals that the localization error captured by $\mathcal{S}_N$, depends critically on the UAV's waypoints. In this section, we formulate the trajectory optimization problem for minimization of the defined localization error. For gaining insights into the solution and defining a performance benchmark, we start with solving the problem in the *offline* setting, assuming that the target position is *known*. The online solution to the optimization problem is postponed to Sec. IV.

A. Problem Formulation

Assume that $\mathcal{S}_N$ and $\mathbf{u}_0$ are given. The offline problem optimizes the UAV's trajectory, namely the sequence of waypoints $\mathbf{u} \triangleq (\mathbf{u}_1, \ldots, \mathbf{u}_N)$, to minimize the worst-case localization error given by the radius of Chebychev circle for $\mathcal{S}_N$. The resulting optimization problem is formulated as

$$\text{P1:} \quad \min_{\mathbf{u} \in \mathcal{U}} \; R_N^2(\mathbf{u}), \tag{11}$$

where $\mathcal{U} = \prod_{n=1}^N \mathcal{U}_n(\mathbf{u}_{n-1})$ and $\mathcal{U}_n(\mathbf{u}_{n-1}) \triangleq \{\mathbf{u}_n \in [0, L_\mathrm{x}] \times [0, L_\mathrm{y}] \mid \|\mathbf{u}_n - \mathbf{u}_{n-1}\| \leq V_\mathrm{max}\Delta_\mathrm{f}\}$ constrains the UAV to fly within the defined rectangular area with a velocity below V_max. The objective function of P1 is given in (10) and can be equivalently reformulated as

$$R_N^2(\mathbf{u}) = \min_{\mathbf{p}_N \in \mathbb{R}^2} \max_{\mathbf{s} \in \mathcal{S}_N} \|\mathbf{s} - \mathbf{p}_N\|^2. \tag{12}$$

Let $\mathbf{s}^*$ and $\mathbf{p}_N^*$ be the optimal solutions of $\mathbf{s}$ and $\mathbf{p}_N$ for problem (12), respectively. Geometrically, $\mathbf{s}^*$ is the intersection of $\mathcal{S}_N$ with its Chebyshev circle centered at $\mathbf{p}_N^*$, cf. Fig. 2.

In problem P1, the objective function value of each given $\mathbf{u}$ is specified via the optimal value of problem (12), which is a convex-nonconcave minimax optimization problem with nonconvex set $\mathcal{S}_N$. Moreover, in problem P1, $\mathcal{S}_N$ is coupled with the UAV's trajectory $\mathbf{u}$. Due to these facts, both problem P1 and problem (12) cannot be optimally solved using existing polynomial-time algorithms. In the following, we first obtain an upper bound on $R_N^2(\mathbf{u})$ using the SDP relaxation technique. Built on this, we then propose an iterative suboptimal solution for problem P1.

B. Problem Transformation

1) Relaxation of Problem (12)*:* Let $\mathbf{W} \succeq \mathbf{s}\mathbf{s}^\mathrm{T}$. Using the auxiliary matrix $\mathbf{W}$, a convex set enclosing the confidence region $\mathcal{S}_N$ is given by

$$\begin{aligned} \hat{\mathcal{S}}_N(\mathbf{W}) = \{\mathbf{s} \in \mathbb{R}^2 \,| I_n^2 \leq \mathrm{Tr}(\mathbf{u}_n\mathbf{u}_n^\mathrm{T} - 2\mathbf{u}_n\mathbf{s}^\mathrm{T} + \mathbf{W}) \leq O_n^2, \\ \mathbf{W} \succeq \mathbf{s}\mathbf{s}^\mathrm{T},\ n = 0, 1, \ldots, N\}, \end{aligned} \tag{13}$$

with $\hat{\mathcal{S}}_N(\mathbf{W}) \supseteq \mathcal{S}_N$, provided $\hat{\mathcal{S}}_N(\mathbf{W}) \neq \emptyset$. Using $\mathbf{W}$ and $\hat{\mathcal{S}}_N(\mathbf{W})$, an upper bound on $R_N^2(\mathbf{u})$ can be derived as

$$R_N^2(\mathbf{u}) \leq \min_{\mathbf{p}_N \in \mathbb{R}^2} \max_{\mathbf{s} \in \hat{\mathcal{S}}_N(\mathbf{W})} \mathrm{Tr}(\mathbf{W}) - 2\mathbf{s}^\mathrm{T}\mathbf{p}_N + \mathbf{p}_N^\mathrm{T}\mathbf{p}_N \tag{14}$$

$$= \max_{\mathbf{s} \in \hat{\mathcal{S}}_N(\mathbf{W})} \min_{\mathbf{p}_N \in \mathbb{R}^2} \mathrm{Tr}(\mathbf{W}) - 2\mathbf{s}^\mathrm{T}\mathbf{p}_N + \mathbf{p}_N^\mathrm{T}\mathbf{p}_N \tag{15}$$

$$= \max_{\mathbf{s} \in \hat{\mathcal{S}}_N(\mathbf{W})} \mathrm{Tr}(\mathbf{W} - \mathbf{s}\mathbf{s}^\mathrm{T}),\ \forall \mathbf{u} \in \mathcal{U}. \tag{16}$$

Here (14) is due to $\hat{\mathcal{S}}_N(\mathbf{W}) \supseteq \mathcal{S}_N$. The right-hand side of (14) is a convex-concave minimax optimization problem with separable optimization variables $\mathbf{p}_N$ and $\mathbf{s}$. Hence, the minimization and maximization in (14) can be interchanged without changing the optimal value [11], which leads to (15). Finally, (16) follows from the fact that $\mathbf{p}_N = \mathbf{s}$ is the optimal solution to the inner minimization problem of (15).

2) Dual of Relaxed Problem (16)*:* Note that (16) is a concave maximization problem and is strictly feasible. Hence, strong duality holds for (16), i.e., it has the same optimal value as its dual problem given in the following lemma.

Lemma 1: For any $\mathbf{u}$, the dual problem of (16) is given as

$$\begin{aligned} \min_{\substack{t\geq 1, \varphi_n \geq 0,\\ \omega_n \geq 0}} \quad & \sum\nolimits_{n=0}^{N} \left[(\omega_n - \varphi_n)\mathbf{u}_n^{\mathrm{T}}\mathbf{u}_n + \varphi_n O_n^2 - \omega_n I_n^2\right] \\ & + \| \sum\nolimits_{n=0}^{N} (\varphi_n - \omega_n)\mathbf{u}_n\|^2/t \\ \text{s.t.} \quad & \sum\nolimits_{n=0}^{N} (\varphi_n - \omega_n) = t, \end{aligned} \tag{17}$$

where φ_n and ω_n are dual variables, and t is an auxiliary variable.

Proof: The derivation is ignored here due to limited page space. Please refer to [11] for a similar proof. ∎

The dual problem (17) is a convex minimization problem. By optimizing $\mathbf{u}$ in (17), problem P1 is reformulated as

$$\begin{aligned} \text{P2:} \min_{\substack{\mathbf{u}\in\mathcal{U}, t\geq 1,\\ \varphi_n \geq 0, \omega_n \geq 0}} \quad & \sum\nolimits_{n=0}^{N} \left[(\omega_n - \varphi_n)\mathbf{u}_n^{\mathrm{T}}\mathbf{u}_n + \varphi_n O_n^2 - \omega_n I_n^2\right] \\ & + \| \sum\nolimits_{n=0}^{N} (\varphi_n - \omega_n)\mathbf{u}_n\|^2/t \\ \text{s.t.} \quad & \sum\nolimits_{n=0}^{N} (\varphi_n - \omega_n) = t, \end{aligned} \tag{18}$$

Like (16), the optimal value of P2 provides an upper bound for that of P1. But unlike (17), the objective function of P2 is not jointly convex with respect to its optimization variables.

C. Trajectory Optimization with Known Target Position

To facilitate a convenient solution for P2, we further relax $\hat{\mathcal{S}}_N(\mathbf{W})$ (or $\mathcal{S}_N$) by setting $I_n \equiv 0$. This leads to $\omega_n \equiv 0$, as the inner bound constraints in $\hat{\mathcal{S}}_N(\mathbf{W})$ (or $\mathcal{S}_N$) are inactive, cf. (8) and Fig. 2. Moreover, define auxiliary variables $\mathbf{z}_n = \varphi_n \mathbf{u}_n \in \mathbb{R}^2$ and let $\mathbf{y}_n \triangleq (\mathbf{z}_n^{\mathrm{T}}, \mathbf{u}_n^{\mathrm{T}}, \varphi_n, t)^{\mathrm{T}}$. Define $\mathcal{Y}_n \triangleq \mathcal{X}_n \times \mathcal{U}_n(\mathbf{u}_{n-1}) \times [0,\infty) \times [1,\infty)$. By considering $I_n \equiv 0$ and using the new notation, problem P2 can be reformulated as

$$\text{P3:} \min_{\mathbf{y}_n \in \mathcal{Y}_n} g(\mathbf{y}_n) + \sum\nolimits_{n=0}^{N} h(\mathbf{y}_n), \tag{19}$$

with nonconvex function $g(\mathbf{y}_n)$ and convex function $h(\mathbf{y}_n)$,

$$\begin{aligned} g(\mathbf{y}_n) \triangleq & \| \sum\nolimits_{n=0}^{N} \mathbf{z}_n\|^2/t + c_1 \sum\nolimits_{n=0}^{N} \|\mathbf{z}_n - \varphi_n \mathbf{u}_n\|^2 \\ & + c_2 \| \sum\nolimits_{n=0}^{N} \varphi_n - t\|^2 \end{aligned} \tag{20}$$

$$\begin{aligned} h(\mathbf{y}_n) = & 2\eta \|\mathbf{z}_n - \varphi_n \mathbf{p}_s\|^3/\varphi_n^2 + \eta^2 \|\mathbf{z}_n - \varphi_n \mathbf{p}_s\|^4/\varphi_n^3 \\ & + \varphi_n \mathbf{p}_s^{\mathrm{T}}\mathbf{p}_s - 2\mathbf{z}_n^{\mathrm{T}}\mathbf{p}_s. \end{aligned} \tag{21}$$

Here, $\eta \triangleq \sqrt{a\sigma^2/(\beta P)}$. $c_1 > 0$ and $c_2 > 0$ are given large penalty factors to prevent non-zero values in $\mathbf{z}_n - \varphi_n \mathbf{u}_n$ and $\sum_{n=0}^{N} \varphi_n - t$.

In Problem P3, though $g(\mathbf{y}_n)$ is a nonconvex function of $\mathbf{y}_n$, it is convex in $(\mathbf{z}_n^{\mathrm{T}}, \varphi_n, t)^{\mathrm{T}}$ for given $\mathbf{u}_n$, and vice versa. Thus, P3 can be solved using the ACO method (similar to steps 4-9 of Algorithm 1), which is guaranteed to converge to a stationary point of P3.

IV. Robust Online Trajectory Optimization

Based on the results of Sec. III, in this section, we further tackle problem P1 in the *online* settings where the target position $\mathbf{p}_s$ is *unknown*, and O_n and I_n, $n = 1, \ldots, N$ are known sequentially after, not before, optimizing waypoint $\mathbf{u}_n$. Instead, $\mathbf{u}_n$ is optimized at each time n, based on the available range measurements or $\mathcal{S}_{n-1}$. We then propose two iterative algorithms to solve P1, which are based on the primal problem (16) and its dual problem P2/P3 in Sec. III, respectively.

A. Proposed Online Algorithm 1

Let $\hat{\mathbf{s}}$ be the optimal solution of problem (16) when the confidence region is given by $\mathcal{S}_{n-1}$. Moreover, let $\hat{\mathbf{p}}_{\text{proj}} \triangleq \mathcal{P}_{\mathcal{S}_{n-1}}(\hat{\mathbf{s}}) = \arg\min_{\hat{\mathbf{p}}\in\mathcal{S}_{n-1}} \| \hat{\mathbf{s}} - \hat{\mathbf{p}}\|^2$ be the projection of $\hat{\mathbf{s}}$ onto $\mathcal{S}_{n-1}$, where SDP relaxation is first used to solve the minimization problem and then, a feasible solution is recovered using the Gaussian sampling technique [16, Ch. 4.2.2]. Based on (15), we use $\hat{\mathbf{p}}_{\text{proj}}$ as a position estimate. Now let $\tilde{d}_n \triangleq \|\mathbf{u}_n - \hat{\mathbf{p}}_{\text{proj}}\|$. Similar to [9], we approximate O_n by,

$$O_n \approx \tilde{O}_n \triangleq \tilde{d}_n + \eta(\tilde{d}_n)^2, \ \forall n. \tag{22}$$

Note that $\tilde{O}_n$ is a convex function of $\mathbf{u}_n$.

To facilitate a tractable solution, we present the online design based on problem P3. By defining $\boldsymbol{\psi}_k \triangleq (\varphi_k, \omega_k)^{\mathrm{T}}$, $k = 0, ..., n-1$, the resulting online problem is formulated as

$$\text{P4:} \min_{\boldsymbol{\psi}_k \geq 0, \mathbf{y}_n \in \mathcal{Y}_n} \sum\nolimits_{k=0}^{n-1} f_0(\boldsymbol{\psi}_k) + \tilde{g}(\mathbf{y}_n, \boldsymbol{\psi}_k) + \tilde{h}(\mathbf{y}_n), \tag{23}$$

in which $\tilde{h}(\mathbf{y}_n)$ is obtained by replacing $\mathbf{p}_s$ with $\hat{\mathbf{p}}_{\text{proj}}$,

$$f_0(\boldsymbol{\psi}_k) \triangleq \left[(\omega_k - \varphi_k)\mathbf{u}_k^{\mathrm{T}}\mathbf{u}_k + \varphi_k O_k^2 - \omega_n I_k^2\right], \tag{24}$$

$$\begin{aligned} \tilde{g}(\mathbf{y}_n, \boldsymbol{\psi}_k) \triangleq & \| \sum\nolimits_{k=0}^{n-1} (\varphi_k - \omega_k)\mathbf{u}_k + \mathbf{z}_n\|^2/t \\ & + c_1\|\mathbf{z}_n - \varphi_n \mathbf{u}_n\|^2 + c_2 \| \sum\nolimits_{k=0}^{n-1} (\varphi_k - \omega_k) + \varphi_n - t\|^2. \end{aligned} \tag{25}$$

Note that $\mathbf{u}_k$, O_k and I_k, $k = 0, \ldots, n-1$, are known. Problem P4 is nonconvex problem due to the nonconvex function $\tilde{g}(\tilde{\mathbf{y}}_k, \boldsymbol{\psi}_n)$. But like P3, P4 can also be solved using the ACO method, which is summarized in Algorithm 1.

B. Proposed Online Algorithm 2

The solution in Sec. IV-A is built on problem P3, the dual problem of (16). Here we present a heuristic solution that is derived based on (16) directly. Let $\mathbf{u}^*$ be the optimal solution of problem P1. We have

$$R_N^2(\mathbf{u}^*) \leq \min_{\mathbf{u}\in\mathcal{U}} \max_{\mathbf{s}\in\hat{\mathcal{S}}_N(\mathbf{W})} \mathrm{Tr}(\mathbf{W} - \mathbf{s}\mathbf{s}^{\mathrm{T}}) \tag{26}$$

$$\leq \min_{\mathbf{u}\in\mathcal{U}} \max_{\mathbf{s}\in\hat{\mathcal{S}}_n(\mathbf{W})} \mathrm{Tr}(\mathbf{W} - \mathbf{s}\mathbf{s}^{\mathrm{T}}), \forall n \leq N \tag{27}$$

$$\leq \min_{\mathbf{u}_n\in\mathcal{U}_n(\mathbf{u}_{n-1})} \max_{\mathbf{s}\in\hat{\mathcal{S}}_n(\mathbf{W})} \mathrm{Tr}(\mathbf{W} - \mathbf{s}\mathbf{s}^{\mathrm{T}}) \tag{28}$$

$$\leq \min_{\mathbf{u}_n\in\mathcal{U}_n(\mathbf{u}_{n-1})} \left(O_n^2 - \|\mathbf{u}_n - \mathbf{s}_{n-1}\|^2\right), \tag{29}$$

Algorithm 1: Online UAV Trajectory Optimization using ACO

initialization: Set $\mathcal{S}_0$ and $\mathbf{u}_0$. Let $n = 1$;
while $n < N$ **do**
  Compute $\hat{\mathbf{p}}_\text{s}$ in problem (16) and $\hat{\mathbf{p}}_\text{proj} = \mathcal{P}_{\mathcal{S}_{n-1}}(\hat{\mathbf{p}}_\text{s})$;
  Set $\mathbf{u}_n^{(0)} \in \mathcal{U}_n(\mathbf{u}_{n-1})$ and iteration index $j = 1$;
  repeat
    Optimize $(\mathbf{y}_n^{(j)}, \psi_k^{(j)})$ for given $\mathbf{u}_n^{(j-1)}$ by solving P4;
    Optimize $\mathbf{u}_n^{(j)}$ for given $(\mathbf{y}_n^{(j)}, \psi_k^{(j)})$ by solving P4;
    Update $j = j + 1$;
  until stopping criterion is met;
  Update $\mathcal{S}_n$ after collecting new measurements at $\mathbf{u}_n$;
  Update $n = n + 1$;
end while

Algorithm 2: Online UAV Trajectory Optimization using SCA

initialization: Set $\mathcal{S}_0$ and $\mathbf{u}_0$. Let $n = 1$
while $n < N$ **do**
  Compute $\hat{\mathbf{p}}_\text{s}$ in (16), $\hat{\mathbf{p}}_\text{proj} = \mathcal{P}_{\mathcal{S}_{n-1}}(\hat{\mathbf{p}}_\text{s})$, and $\mathbf{s}_{n-1}$;
  Set $\mathbf{u}_n^{(0)} \in \mathcal{U}_n(\mathbf{u}_{n-1})$ and iteration index $i = 1$;
  repeat
    $\mathbf{u}_n^{(i)} = \arg\min_{\mathbf{u}_n \in \mathcal{U}_n(\mathbf{u}_{n-1})} f_1(\mathbf{u}_n) - [f_2(\mathbf{u}_n^{(i-1)}) + \nabla f_2(\mathbf{u}_n^{(i-1)})(\mathbf{u}_n - \mathbf{u}_n^{(i-1)})]$;
    Update $i = i + 1$;
  until stopping criterion is met;
  Update $\mathcal{S}_n$ after collecting new measurements at $\mathbf{u}_n$;
  Update $n = n + 1$;
end while

where (26) restates the result in (16) as a convex-concave minimax problem. As $\mathbf{u}$ and $\mathbf{s}$ are coupled in (26), the approach in Sec. III-B cannot be employed to solve (26). Instead, we derive a computable upper bound for (26) via inequalities (27)–(29), where (27) is due to $\hat{\mathcal{S}}_n(\mathbf{W}) \supseteq \hat{\mathcal{S}}_N(\mathbf{W})$, $\forall \mathbf{u}$, $\forall n \le N$. In (28), we define $\overline{\mathcal{S}}_n(\mathbf{W}) \triangleq \{\mathbf{s} \in \hat{\mathcal{S}}_n(\mathbf{W}) \mid \mathbf{u}_1, \ldots, \mathbf{u}_{n-1} \text{ are given}\}$ and the inequality holds since fixing $\mathbf{u}_1, \ldots, \mathbf{u}_{n-1}$ is suboptimal. Finally, (29) is due to

$$
\begin{aligned}
&\max\nolimits_{\mathbf{s} \in \overline{\mathcal{S}}_n(\mathbf{W})} \operatorname{Tr}(\mathbf{W} - \mathbf{s}\mathbf{s}^\text{T}) \\
&\le \max\nolimits_{\mathbf{s} \in \overline{\mathcal{S}}_{n-1}(\mathbf{W})} \operatorname{Tr}(\mathbf{W} - \mathbf{s}\mathbf{s}^\text{T}) && (30) \\
&\le \max\nolimits_{\mathbf{s} \in \overline{\mathcal{S}}_{n-1}(\mathbf{W})} O_n^2 - \mathbf{u}_n^\text{T}\mathbf{u}_n + 2\mathbf{u}_n^\text{T}\mathbf{s} - \mathbf{s}^\text{T}\mathbf{s} && (31) \\
&= O_n^2 - \|\mathbf{u}_n - \mathbf{s}_{n-1}\|^2, \ \ \forall \mathbf{u}_n \in \mathcal{U}_n(\mathbf{u}_{n-1}), && (32)
\end{aligned}
$$

where (31) is due to (13) and $\mathbf{s}_{n-1}$ is its optimal solution.

In general, the upper bound in (29) can be quite loose. To tighten the bound, we choose to recover a rank-one solution of $\mathbf{W}$ based on its optimal solution in (30) using the Gaussian sampling [16, Ch. 4.2.2]. Based on this, we then select $\mathbf{s}_{n-1}$ as the intersection of $\overline{\mathcal{S}}_{n-1}(\mathbf{W})$ with its Chebyshev circle, which is an extreme point of $\overline{\mathcal{S}}_{n-1}$. By approximating O_n as in (22), the objective function of problem (29) is given as a difference of convex functions $f_1(\mathbf{u}_n) = (\|\mathbf{u}_n - \hat{\mathbf{p}}_\text{proj}\| + \eta\|\mathbf{u}_n - \hat{\mathbf{p}}_\text{proj}\|^2)^2$ and $f_2(\mathbf{u}_n) = \|\mathbf{u}_n - \mathbf{s}_{n-1}\|^2$. Therefore, problem (29) can be sovled using the SCA method, as given in Algorithm 2.

V. Simulation Results

In this section, we evaluate the performance of the proposed schemes via simulations. We consider a rectangular area of dimension $L_\text{x} = L_\text{y} = 1000$ m, while the target is located at $\mathbf{p}_\text{s} = [900, 600]^\text{T}$. The UAV takes off at $[0, 50]^\text{T}$. Having this initial confidence region, we compute an initial estimated position of target. After that, the UAV starts to design its trajectory either using offline optimization or online optimization approaches. The other simulation parameters are given in Table I. For providing performance benchmarks, we also evaluate two baseline schemes,

- *Baseline Scheme 1*: The UAV knows the target position $\mathbf{p}_\text{s}$ and optimizes its trajectory offline as in Sec. III-C.

TABLE I: Simulation Parameters

Parameter	**Value**
UAV's flight altitude	$h = 100$ m
Transmit power of sensing signal	$P = 0.5$ W
Power gain factor	$\beta = -50$ dB
Received noise power	$\sigma^2 = -110$ dBm
System parameter in (4)	$a = 1$
Maximum flight velocity	$V_\text{max} = 30$ m/s
Maximum number of waypoints	$N = 15$
Number of measurements per waypoint	$M = 41$
Confidence level	$\alpha\% = 99\%$
Flight duration between waypoints	$\Delta_\text{f} = 4$ s

- *Baseline Scheme 2*: The UAV employs the online Algorithm 2 to optimize the next waypoint, but it can only fly in 4 (left, right, up, and down) directions or hover.

For initializing the considered schemes, the UAV obtains an initial confidence region of localization $\mathcal{S}_0$ by flying and measuring the range over $N_\text{init} = 3$ predefined waypoints, with the last waypoint being $\mathbf{u}_0$.

Fig. 3 and Fig. 4 show the UAV trajectories, the worst-case localization errors, and distances $\|\hat{\mathbf{p}}_\text{proj} - \mathbf{p}_\text{s}\|$ at each waypoint, respectively. We observe that, with the Baseline Scheme 1, the UAV flies almost in a straight line towards the target for $n \le 7$, and the resulting localization error significantly decreases over time. This is because, with the target position known at the UAV, approaching the target can lower the error variances of range measurements at each waypoint, and further reduce the worst-case localization error. However, the UAV tends to circle around the target, instead of approaching it, for $n \in \{7, \ldots, N\}$. This is because the UAV is close to the target and the error variances of range measurements are small. By circling around the target, the UAV can exploit multi-lateration at different angles to further improve the localization.

Meanwhile, the proposed online scheme 2 aims to minimize an upper bound of the optimal value, defined based on the extreme point $\mathbf{s}_{n-1}$, cf. (29). From Fig. 3 and Fig. 4 we observe that, as the initial extreme point is far from the target estimate, the UAV circles around the extreme point, which intends to exclude the extreme point from the confidence region using the range measurement that would be collected at the next waypoint. Nevertheless, due to the loose upper

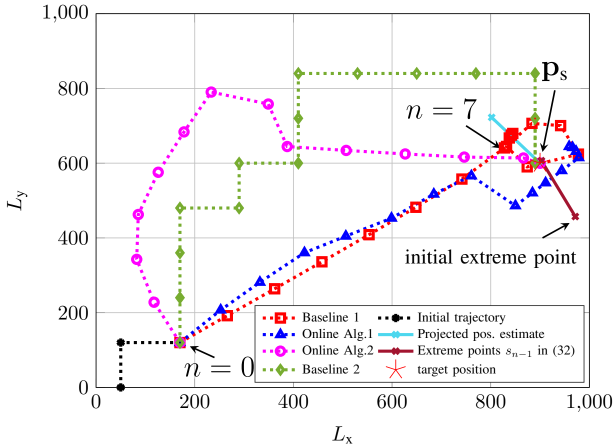

Fig. 3: Comparison of the UAV's flying trajectories.

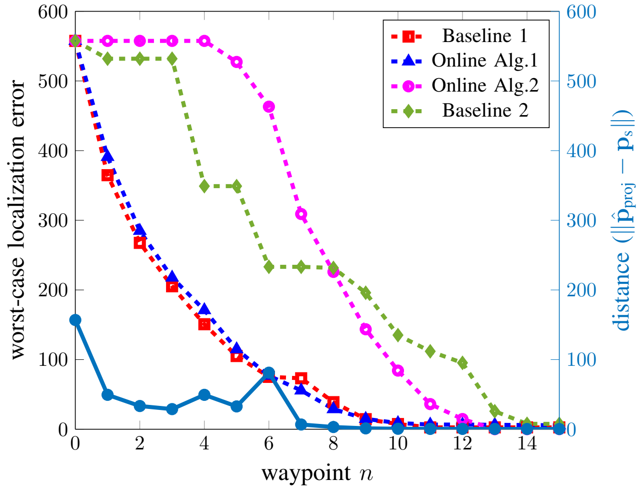

Fig. 4: Worst-case localization errors and distances $\|\hat{\mathbf{p}}_{\text{proj}} - \mathbf{p}_s\|$ along waypoints.

bound in (29), the worst-case localization error saturates for $n \in \{0, \ldots, 4\}$. In contrast, when the extreme point is close to the target estimate, the UAV starts approaching the target estimate. It is interesting to see that the resulting localization error of the proposed online Algorithm 2 decreases over $n \in \{4, \ldots, 12\}$ even faster than that of the proposed online Algorithm 1 does over $n \in \{0, \ldots, 10\}$. On the other hand, due to quantization of flight directions, the UAV's trajectory of the Baseline Scheme 2 deviates from that of the proposed online scheme 1, with random effects on the localization performance.

Fig. 4 shows that the proposed online scheme 1 outperforms the other online localization schemes, namely the proposed online scheme 2 and the Baseline Scheme 2, where both the flying trajectory and localization performance of the proposed online scheme 1 are close to that of the Baseline Scheme 1. The former is because both the proposed online scheme 2 and the Baseline Scheme 2 employ the loose upper bound in (29). On the other hand, the latter is because as shown in Fig. 4, the differences between the projected position estimates $\hat{\mathbf{p}}_{\text{proj}}$ and the target position $\mathbf{p}_s$ are much smaller, compared to the worst-case localization error, and become negligible after flying over 7 waypoints.

VI. Conclusion

This paper considered robust dynamic trajectory optimization for UAV-aided localization, to minimize the proposed (probabilistic) worst-case localization error metric. The latter characterizes the radius of the Chebyshev circle for the α-confidence region of localization. Two iterative online sub-optimal algorithms designed based on SDP relaxation and the ACO/SCA methods were further proposed to tackle the intractable problem. Simulation results showed that, compared to several baselines, the proposed online algorithms can effectively exploit the movement of the UAV to achieve either the best overall localization performance or the fastest rate of decrease in the localization error. In this paper, we have assumed that the target remains in the UAV's LoS sensing range and that the errors in range estimation follow Gaussian distributions. Modifying or omitting these assumptions in real-world contexts is a promising direction for future research.

References

[1] N. H. Motlagh, T. Taleb and O. Arouk, "Low-Altitude Unmanned Aerial Vehicles-Based Internet of Things Services: Comprehensive Survey and Future Perspectives," *IEEE Internet Things J.* vol. 3, no. 6, pp. 899-922, Dec. 2016.

[2] A. Wang, X. Ji, D. Wu, et al., "Guideloc: UAV-assisted multitarget localization system for disaster rescue", *Mobile Inf. Syst.*, vol. 2017, pp. 1–13, Mar. 2017.

[3] B. Yuan, R. He, B. Ai, et al., "A UAV-assisted search and localization strategy in non-line-of-sight scenarios", *IEEE Internet Things J.*, vol. 9, no. 23, pp. 23841–23851, 2022.

[4] F. B. Sorbelli, S. K. Das, C. M. Pinotti, et al., "Range based algorithms for precise localization of terrestrial objects using a drone," *Pervasive Mobile Comput.*, vol. 48, pp. 20–42, 2018.

[5] I. Guvenc and C. -C. Chong, "A Survey on TOA Based Wireless Localization and NLOS Mitigation Techniques," *IEEE Commun. Surveys Tut.*, vol. 11, no. 3, pp. 107-124, 3rd Quarter 2009.

[6] H. Kwon and I. Guvenc, "RF signal source search and localization using an autonomous UAV with predefined waypoints", *arXiv preprint arXiv:2301.07027*, 2023

[7] C.-S. Chen, Y.-J. Chiu, C.-T. Lee, et al., "Calculation of Weighted Geometric Dilution of Precision", *J. Appl. Mathematics*, 2013.

[8] S. Jayasekara, A. Al-Hourani, B. Risti, et al., "Autonomous UAV Search for an RF Source in Urban Environments", in *Proc. ICSPCS*, 2020.

[9] X. Jing, F. Liu, C. Masouros, et al., "ISAC from the sky: UAV trajectory design for joint communication and target localization", *arXiv preprint arXiv:2207.02904*, 2022.

[10] M. Kay. *Fundamentals of Statistical Signal Processing: Estimation Theory*. Prentice Hall, 1997.

[11] X. Shi, G. Mao, B. D. Anderson, et al., "Robust Localization Using Range Measurements With Unknown and Bounded Errors," *IEEE Trans. Wireless Commun.*, vol. 16, no. 6, pp. 4065-4078, Jun. 2017.

[12] S. Zhao, X.-P. Zhang, X. Cui et al., "Optimal Two-Way TOA Localization and Synchronization for Moving User Devices With Clock Drift," *IEEE Trans. Veh. Technol.*, vol. 70, no. 8, pp. 7778-7789, Aug. 2021.

[13] M. A. Richards. *Fundamentals of Radar Signal Processing*. McGraw-Hill Education, 2014.

[14] P. Sinha and I. Guvenc, "Impact of Antenna Pattern on TOA Based 3D UAV Localization Using a Terrestrial Sensor Network," *IEEE Trans. Veh. Technol.*, vol. 71, no. 7, pp. 7703-7718, Jul. 2022.

[15] E. W. Weisstein, "Student's t-Distribution", MathWorld–A Wolfram Web Resource. [Online] Avilable: https://mathworld.wolfram.com/Studentst-Distribution.html.

[16] D. Palomar and Y. Eldar (Eds.). *Convex Optimization in Signal Processing and Communications*. Cambridge University Press, 2009.